USBL Integration and Assessment in a Multisensor Navigation Approach for AUVs ⋆

Eric Guerrero Font * Francisco Bonin-Font * Pep-Lluis Negre *
Miquel Massot * Gabriel Oliver *

* Systems, Robotics and Vision Group. University of the Balearic
Islands, Cra. Valldemossa, km. 7,5 , 07122 Palma de Mallorca (Spain)
(e-mail: ericguerrerofont@gmail.com, francisco.bonin@uib.es ,
pl.negre@uib.cat, miquel.massot@uib.cat, goliver@uib.es

Abstract: This paper presents the design and assessment of an USBL-aided navigation approach for *Autonomous Underwater Vehicles* (AUV). The system integrates an *Ultra-Short Base Line* (USBL) acoustic modem and positioning device in a two-parallel *Extended Kalman Filter* (EKF) navigation schema, which also includes the measurements provided by an *Inertial Measurement Unit* (IMU), a *Doppler Velocity Log* (DVL), a *Visual Odometer* (VO), a pressure sensor, and a *Global Positioning System* (GPS). In order to be integrated in the estimation filter, the precision of the USBL measurements is derived experimentally. Moreover, the accuracy of the system is evaluated using a ground truth (GT) trajectory produced by a visual *Simultaneous Localization and Mapping* (SLAM) approach. Experimental results are obtained from marine datasets gathered in the north coast of Mallorca with an AUV, model SPARUS II.

Keywords: Robotics, Localization, Navigation, USBL, AUV.

1. INTRODUCTION

Advances in marine research have let the scientific community to improve underwater robots with higher autonomy and better on-board sensor suites, enabling more complex and longer tasks. Missions addressed to deep waters are usually carried out by *Remotely Operated Vehicles* (ROV), requiring costly infrastructures and specialized personnel. However, lightweight and low-cost AUVs require lower and much cheaper equipment, offering higher dependability.

Autonomous navigation and intervention underwater requires accurate and precise localization. Due to the absence of GPS underwater, localization approaches are usually based on odometric and inertial sensors, which produce trajectory drift. A possible solution to correct this drift is detecting loop closings (the vehicle passes over an already visited region). That's the case of the visual SLAM approaches specialized in challenging underwater environments (Negre et al., 2016). However, loop closing detection is not always technically possible due to the nature of the mission or the environmental conditions.

A reliable alternative to underwater global positioning is the use of absolute-sensing devices, such as, pressure sensors or acoustic transponders as *Long Base Line* (LBL) (Willemenot et al., 2009) or USBL. While an LBL system requires the deployment of at least three transponders at known positions to triangulate the position of a fourth, the USBL requires the deployment of only one device which is composed of a transponder and an hydrophone array used to triangulate a mobile target transponder. In addition, the USBL can incorporate an *Attitude Heading Reference System* (AHRS) and a GPS, to reference the measurements relative to a world reference frame. Besides, the USBL permits an acoustic low-rate communication with the moving vehicle, which can be used to exchange navigation and localization data. Although USBLs offer communication at low rates ($\sim kbps$), they can establish links at large ranges ($\sim km$).

The precision and accuracy are important technical indexes of the USBLs, but there is not an unified method to measure them due to the difficulty of obtaining a reliable GT in a marine scenario. Accuracy reflects how close a measurement is to a certain value accepted as a GT while the precision reflects how reproducible are the measurements, although they are far from the GT. Some authors approach the problem of the USBL precision evaluation assuming the error ellipse theory and that the USBL measurements with the added errors follow a Gaussian distribution (Sun et al., 2014). Some other authors (Rigby et al., 2006) conclude that the overall positioning measurements considering USBL, GPS and AHRS do not follow a normal distribution due to the inevitable existence of system errors, becoming non-linear processes with added non-Gaussian noise. This complicates enormously the formalization of the USBL error affecting the vehicle localization, imposing a more practical and experimental assessment.

The position of the mobile transponder calculated by the USBL head can be sent to the vehicle using the acoustic

communication channel. Once it reaches the robot, the position can be used for navigation and control. However, using only the USBL positioning for AUVs navigation is not feasible due to: a) the delay in the localization data caused by the high latency of the acoustic communication link, and b) the low frequency in the position data emission. Consequently, the best solution is fusing multiple sensors (inertial, visual, DVL and USBL) in a Kalman Filter to: a) reduce the uncertainty in localization with multiple and redundant sources of information, and b) feed the control and navigation modules with diverse data provided at different frequencies. Several navigation solutions formalize explicitly the formulation of the USBL measurement delays to integrate them in a *Delayed State Information Filter* (DSIF) (Ribas et al., 2012) or in an *Unscented Kalman Filter* (Stanway, 2010). Instead, we simplify the process by including implicitly the delay in the USBL position sample, maintaining the traditional EKF mathematical structure.

Robust and reliable localization modules are critical for the two Spanish national projects, ARSEA (TIN2014-58662-R) and SUPERION (DPI2014-57746-C3), where underwater multi-robot cooperation and multi-modal perception systems aim to boost the progress in underwater exploration, mapping and intervention. The present paper presents the design and performance of an USBL-aided navigation module for underwater robots based on two different filters; one filter returns the vehicle odometry, the other filter provide us with the vehicle global pose. While the former obtained from the inertial and dead-reckoning sensors, the latter is obtained with the same inputs plus the GPS (when the vehicle is in the surface) and the USBL measurements. The output of the odometry filter is key to compensate the delay of the USBL samples inherent to its high latency, and to filter USBL outliers.

The contributions of this paper are relevant in twofold. Firstly, section 2 presents an evolution of the original SPARUS II navigation architecture. Starting with a remainder about Kalman filtering in secction 2.1, and moving on the description of the USBL measurement update and outlier rejection to enable the integration of an USBL delayed measurement in an absolute estimation filter in sections 2.2 and 2.3. Secondly, it provides an experimental evaluation of the USBL integration performance; providing the USBL measurements precision in section 3.1, and the assessment of the global localization system accuracy compared with a visual SLAM localization algorithm as a GT in section 3.2.

2. NAVIGATION AND USBL INTEGRATION

The architecture of the vehicle implements an evolved multi-layer software structure developed under the ROS middleware (Quigley et al., 2009) and formed by a navigation, a control, a guidance and a safety layers (Guerrero et al., 2016). The sensor aggregator node, located in the navigation layer, has 4 main functions: 1) centralizing the reception of all the sensor measurements, 2) checking their reliability and if they are provided accordingly to the required frequency demands, 3) transforming the data streams into formatted poses (velocity, odometry or IMU messages), and 4) assuring the correct robot initialization

setup, allowing the activation of thrusters and further mission operation only if all navigation sensors have been correctly plugged and configured.

2.1 Kalman filters

The new navigation module implements two Kalman Filters. In the first filter, (called *ekf_odom*), predictions are computed using kinematics and an update is made every time a sample is provided by different medium-hight frequency sensors: the velocity given by a DVL and a visual feature tracker, the rotation rates provided by the IMU, and the position updates in z from the depth sensor. Although this odometry is accurate for a short term motion estimation, it presents a considerable drift when integrated to compute the vehicle trajectory. The second filter (called *ekf_map*) uses the same inputs of the *ekf_odom* plus the GPS and the USBL data, which provide global positioning samples at a lower frequency. As described in section 2.2, the vehicle odometry, *ekf_odom*, will be essential to update the delayed position measurements.

Both EKFs have been implemented with the *robot localization* ROS package (Moore and Stouch, 2016), since it offers EKFs and *Unscented Kalman Filters* (UKFs) (Julier and Uhlmann, 1997) in a completely versatile and configurable standard ROS package. The 15-dimensional state vector in both EKFs is formed by the pose $(x, y, z, roll, pitch, yaw)$, the linear and angular velocities $(v_x, v_y, v_z, w_x, w_y, w_z)$ and the linear accelerations (a_x, a_y, a_z). The prediction step of both EKFs is characterized as: $x_k = f(x_{k-1}) + w_{k-1}$ and $\hat{P}_k = FP_{k-1}F^T + Q$, where x_k is the state vector at time k, f is a non-linear state transition function, w is the normally distributed process noise, P_k is the covariance of the predicted state and F is the Jacobian of f(x_k). In our case, f denotes the composition in 6DOF of the last vehicle position with the last odometry measurement. Measurements can be modelled as: $z_k = h(x_{k-1}) + v_{k-1}$, where z_k is the real sensor measurement at time k, h is the non-linear observation sensor model function, and v_k is the normally distributed measurement noise. The process noise covariance Q is a parameter tuned by the user. Finally, the updating equations can be formulated as: $K = \hat{P}_k H^T (H\hat{P}_k H^T + R)^{-1}$, $x_k = \hat{x}_k + K(z - H\hat{x}_k)$ and $P_k = (I - KH)\hat{P}_k(I - KH)^T + KRK^T$, being K the filter *gain*, H the Jacobian of $h(x_k)$, and R the measurement noise covariance matrix. To support a broad array of sensors, the Jacobian of the observation model (H) is simply set to the identity matrix (Moore and Stouch, 2016).

2.2 Measurement update

In a typical configuration, the USBL head estimates the (x, y, z) position of the AUV transducer, relative to the USBL reference frame. The USBL is usually connected to a surface station, and has a GPS attached which permits to transform the vehicle USBL coordinates to the world reference frame. Afterwards, these global position can be sent acoustically to the vehicle for navigation and control. However, due to the high latency inherent to the acoustic communications, the USBL position updates might be transmitted to the vehicle with a significant delay (order of seconds), and thus incorrectly integrated into the *ekf_map*.

In consequence, accurate localization requires an update of the USBL measurements received in the vehicle.

The measurement update is performed as follows:

- At the ground station, a series of geometric transformations are performed to convert the relative position that the USBL head produces into an absolute reference frame, using the geodetic location of the device provided by the USBL attached GPS module.

$$T_{map}^{sparus} = T_{map}^{usbl} \cdot T_{usbl}^{sparus} \tag{1}$$

  The measurements are transformed to a */map* frame fixed to the world following the *North, East, Down (NED)* convention. And Frames */usbl* and */sparus* are fixed to the USBL head and the AUV, respectively. T_{map}^{usbl} and T_{usbl}^{sparus} are the transforms provided by the GPS and USBL measurements, respectively. These measured vehicle global positions and their time stamps are then sent acoustically to the AUV.

- In the robot, the received absolute USBL measurement (which is delayed due the high communication latency) is updated by composing it with the vehicle displacement estimated by the odometric filter, *ekf_odom*, after the USBL measurement was produced. Then, the updated absolute measurement is fed to the absolute filter *ekf_map*.

Figure 1 shows all the coordinate frames related to the measurement update. They are presented in two different time instants; the instant in which the measurement was produced, t_0, and the instant in which the measurement arrives to the robot, t_1. s_0' and s_1' represent the vehicle positions estimated by the USBL referenced to the USBL frame at both time instants, $usbl_0$ and $usbl_1$. The difference between *ekf_map* and *ekf_odom* returns the odometric trajectory drift, which is used by the robot coordinate transformation tree as the transform T_{map}^{odom}. Being */odom* defined as the frame that refers the odometric drift with respect to */map*. s_0 and s_1 represent the odometric vehicle pose given by *ekf_odom* filter, since the */odom* frame position depends on time, they are given with respect to $/odom_0$ and $/odom_1$, respectively.
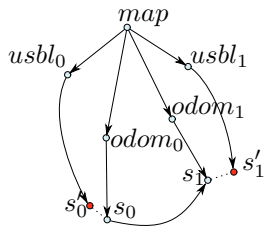

Fig. 1. USBL synchronization

We assume that the updated USBL vehicle position is equal to the delayed USBL vehicle position composed with the vehicle displacement estimated by the odometry. Let be $\Delta odom = T_{s_0'}^{s_1'}$, then, the non-delayed USBL position of the robot can be estimated as $T_{map}^{s_1'} = T_{map}^{usbl} \cdot T_{usbl_0}^{s_0'} \cdot \Delta odom$.

Since, by definition, $\Delta odom$ is the difference of both odometric estimations, equation 2 provides the update of the USBL measurement.

$$T_{map}^{s_1'} = T_{map}^{usbl_0} \cdot T_{usbl_0}^{s_0'} \cdot T_{odom_1}^{s_1'} \cdot T_{s_0}^{odom_0'} \tag{2}$$

2.3 Outlier rejection

Furthermore, before feeding the localization filter with the USBL measurements, an outlier rejection technique is applied. Some measurements are considered outliers and rejected if the difference between the movement measured by the USBL during the last two received samples and the movement estimated by the *ekf_odom* is higher than a certain threshold during the same period. The threshold will depend on the vehicle speed.

2.4 Software architecture

Figure 2-(a) illustrates the ROS software structure used in the ground station (GS) to calculate the delayed vehicle global position from the USBL measurements.
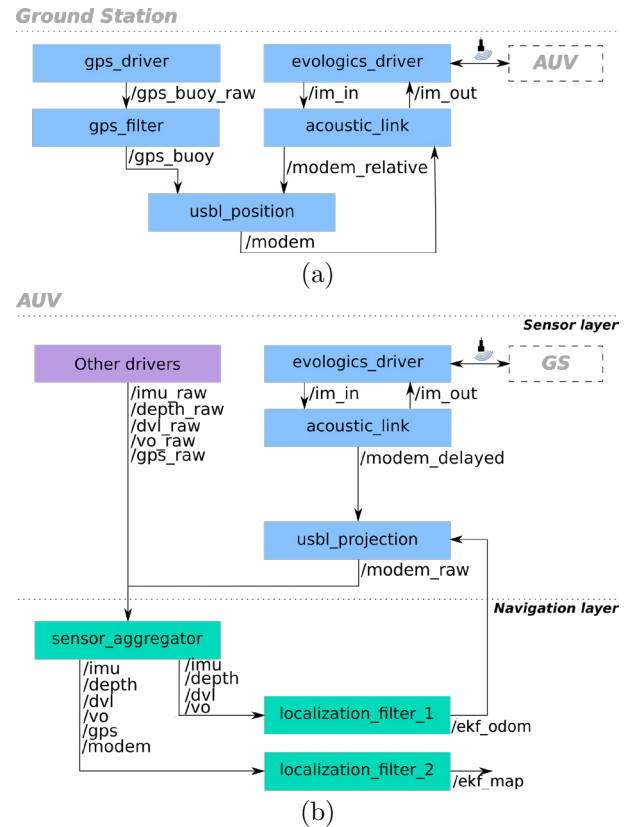

Fig. 2. Schema of the acoustic driver in the (a) Ground Station, and (b) in the AUV.

At the GS the GPS driver node provides the geodetic location of the USBL head, it is published in the (*/gps_buoy_raw*) topic and then filtered in a different node. The *evologics_driver* node captures the USBL raw measurements (vehicle position relative to the USBL head) and inputs them into the *acoustic_link* node. This node is the bridge between the USBL driver and the ROS architecture, and transforms the message structure to a

ROS standard pose message (/*modem_relative*). Finally, the node *usbl_position* composes the vehicle positions relative to the USBL with the filtered GPS to obtain the vehicle global position(/*modem*) as stated in equation 1. Then the messages of the /*modem* topic are transformed by the *acoustic_link* node to output them to the *evologics_driver*, and finally be sent to the AUV via the acoustic modem.

In the AUV architecture (figure 2-(b)) the USBL driver node *evologics_driver* receives the input messages via acoustic communication and sends them to the *acoustic_link* node, which transforms them into a standard ROS pose messages (/*modem_delayed*). The node *usbl_estimation* transforms the position contained in the /*modem_delayed* message using the odometry data according to the process described in section 2.2 to minimize the USBL delay effect. It performs the transformation of equation 2. Afterwards, the corrected vehicle global position (*modem_raw*) together with the other sensor data are used as an input for the navigation filters. It is important to realize that the odometry estimation, *ekf_odom*, is key to update the USBL measurements. However, the absolute localization will be provided by the absolute estimation of *ekf_map*.

This library is available to the scientific community in a public repository under the GNU license (Negre and Guerrero, 2016).

3. EXPERIMENTS

A first set of broad experiments were conducted at several points of the north coast of Mallorca, with good weather conditions. The AUV SPARUS II was equipped with a stereo rig, a DVL, an IMU, a pressure sensor and an Evologics S2CR 18/34 USBL acoustic modem which provides a communication link with bit rate up to 13.9*kbps*, and an available communication range up to 3500*m* in open waters. The USBL head was mounted on a buoy with a GPS attached on its top, and linked to a laptop located on a port breakwater through Ethernet connection. The USBL buoy was properly moored to the sea bottom in order to limit its motion caused by the sea currents (figure 3). The USBL vehicle position was converted to a global NED referenced position using the USBL AHRS and the GPS buoy estimations, and sent acoustically to the vehicle to be integrated in the *ekf_map*. Additionally, the acoustic link was also used to send *services* from the laptop to the vehicle (such as *lights on/off*, *emergency surface* or *disable thrusters*) and to receive navigation and status data in the laptop from the vehicle (i.e. *filtered pose data* and *battery voltage*). These experiments were performed on shallow coastal waters, ∼ 6*m*, where the working conditions for the USBL are always worse than in open sea, due to the acoustic multipath propagation caused by the ground, water surface, rocks or even the breakwater.

3.1 Precision test

In a sample experiment, the AUV was programmed to conduct a rectilinear path with a set of way-points distributed evenly every 15m; at 34m, 51m, 66m, 81m and 96m from the USBL head. At every way-point the robot was programmed to perform a hovering maneuver, maintaining
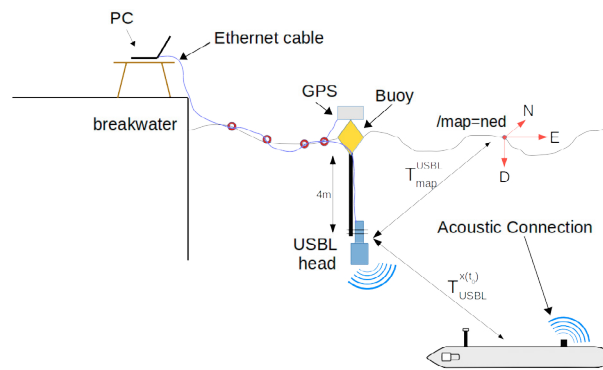

Fig. 3. Experimental Setup Schema

its pose during 90 seconds. The horizontal USBL vehicle positioning was recorded during the whole route, as well as the output of the odometric filter. The data collected at each way-point was used to calculate the measurement precision. The slight motion of the vehicle due to hovering errors and the lack of the lateral degree of freedom was estimated by the *ekf_odom* in order to correct the usbl measurements and analyze the data as if the vehicle was static. This precision should give a measure of confidence about the USBL position estimates, which could be used in further tests by the absolute positioning filter *ekf_map* as the uncertainty associated to the measurement.

Figure 4 shows the vehicle trajectory and the obtained USBL measurements during the hovering period of the third way-point, at 66*m*.
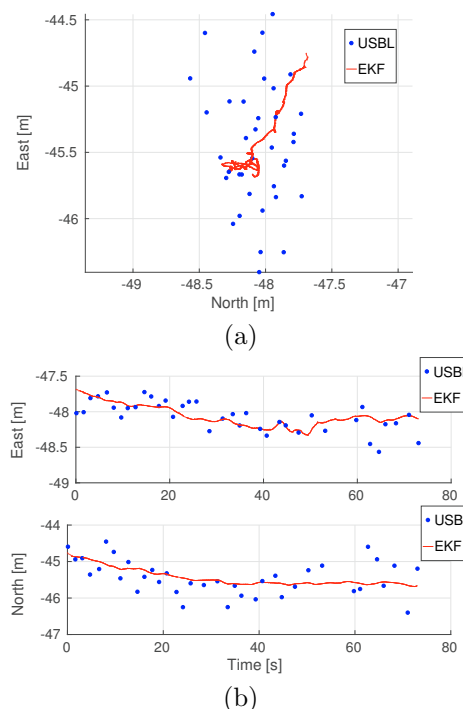

Fig. 4. USBL measures and odometric trajectory estimation during the hovering period of the third way-point; (a) horizontal and (b) time series representations.

The trajectory is estimated by the *ekf_odom* filter, which integrates visual odometry estimations obtained from a downward stereo pair. It can be considered as the tra-

jectory GT, since the drift caused by the small movement produced in 90s might be negligible when compared to the USBL noise. Only the horizontal coordinates have been represented in this plot, since the vertical component of the USBL will not be used in the filter integration; it is very noisy in shallow waters and the depth sensor already produces a rather good estimation.

The error dispersion of the USBL position data is obtained as the distance between the odometric trajectory (the GT) and the USBL measurements trajectory. One error sample is obtained from the distance between an USBL measurement an the GT position for the same instant. The error samples are supposed to capture the USBL error dispersion with respect a GT. Then, we used the maximum eigenvalue (λ_{max}) of the each resulting point dispersion, for each hovering way-point, to get measurement variance in the maximum direction of dispersion. The error distribution for each hovering way-point is represented in 5-(a). Figure 5-(b) shows the λ_{max} obtained at each distance of the USBL head; a linear regression is inferred from them, $y = 0.0023x - 0.0148m$, which evidences that the precision of the system decreases with the distance.
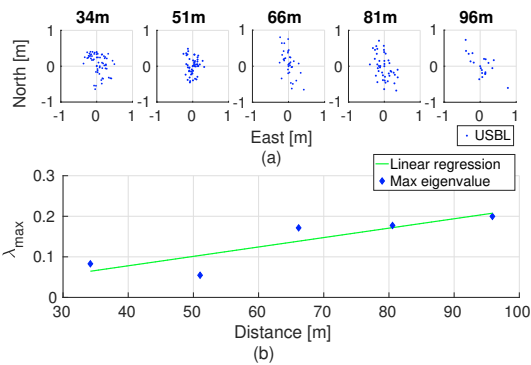

Fig. 5. USBL position error; (a) dispersion and (b) linear regression.

During the first $100m$ the maximum value of λ_{max} is $0.2m$. Since $\lambda_{max} = \sigma^2$, the standard deviation is thus $\sigma = 0.45m$. Furthermore, the linear regression of the maximum eigenvalues provides a numerical estimation of the precision in the studied distance range $[34, 96]m$, increasing with the distance.

The precision estimated experimentally was used to set a value to the USBL measurement covariance. Primarily to be used by the *ekf_map* filter as the degree of believe over the measure. Although the analysis of a longer dataset with more way-points would definitively complement or augment the accuracy of the obtained results, the formulated linear regression let us to approximate the uncertainty of the USBL measurements up to a $100m$ distance range, in shallow coastal waters.

3.2 Accuracy test

Another set of experiments was performed to asses the AUV localization accuracy. In order to do so, the visual SLAM approach proposed by (Negre et al., 2016) was used as a GT. Which demonstrated robustness on underwater

scenarios, and guaranted the absence of drift and reliability even in marine areas poor in features. Furthermore, the presented test was performed in best case scenario conditions for underwater imaging, in a feature rich sea bottom with proper natural lighting, avoiding most of the typical image perturbations such as flickering and scattering. The AUV performed a rectangular grid-shaped survey mission, $15m \times 15m$, $270m$ long, covering an approximated area of $225m^2$. In this set of experiments, the *ekf_odom* filter did not integrate visual odometry, only DVL, IMU and pressure sensor. And the *ekf_map* included the USBL, and the GPS in case of being at the surface.

Figure 6 shows the GT trajectory estimated by the stereo SLAM algorithm, and the estimations of both filters, odometric and absolute. The odometric trajectory shows a significant drift, while the *ekf_map* fits better the GT. Furthermore, figure 7 shows the time series, in the *north* and *east* axis.
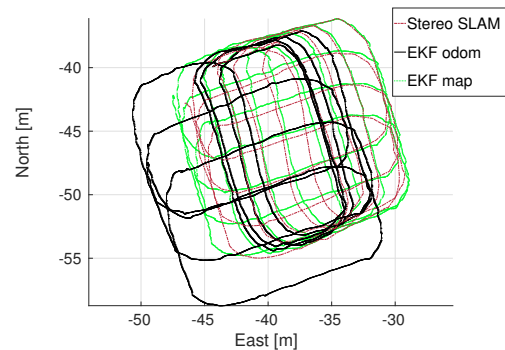

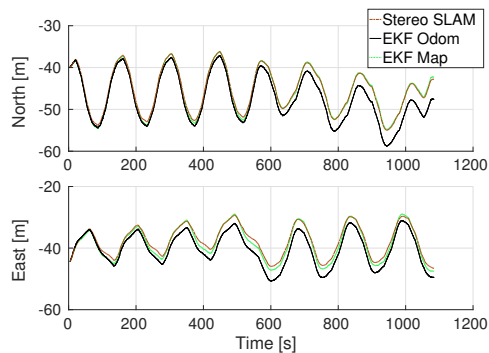Fig. 6. Robot trajectory estimated by the Stereo SLAM, the *ekf_odom* and the *ekf_map*.

Fig. 7. Robot trajectory in the *north* and *east* axis.

Figure 8 shows the trajectory error, computed as the euclidean distance between the different pose estimators with respect to the GT, for the horizontal position. Since the time stamp of each stereo SLAM node was out-of-time with respect to the time stamp of each EKF state, a previous process of sample interpolation was necessary to estimate a pose value of the SLAM trajectory just at each EKF state time stamp. From the figure 8 can be deduced that: a) the *ekf_map* presents the lowest trajectory error, b) the trajectory error corresponding to the *ekf_odom* grows unbounded as the vehicle moves, and c) the trajectory errors of the *ekf_map* and the USBL positioning samples are bounded, limited between $[0, 2.8]m$. The mean and standard deviation of trajectory error for the *ekf_odom* and

of the *ekf_map* turned out to be $\mu_{odom} = 3.4m$, $\sigma_{odom} = 1.3m$, $\mu_{map} = 0.89m$ and $\sigma_{map} = 0.48m$. Remember that the dispersion obtained in the precision test was upper bounded by $\sigma = 0.45m$. Taking into account that the accuracy test has been performed closer to the USBL head $\sim 15m$, the obtained σ_{map} would be expected to be smaller. The increased value may be caused by some aditional noise introduced by the filter or by the GT.
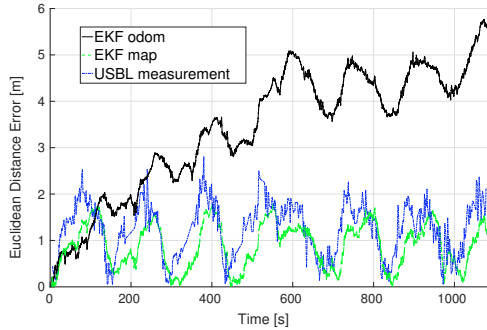

Fig. 8. Trajectory errors of both filters and the USBL.

3.3 EKF and UKF comparison

Since EKFs are, in principle, only reliable for systems which are nearly linear on the time scale of the filter update intervals (Julier and Uhlmann, 1997), and UKFs are claimed to improve the localization performance when the model transitions are highly non-linear, the presented localization module was tested also with UKFs. Figure 9 shows the trajectory error versus time, with respect to the stereo SLAM estimates, of the *ekf_map* and the *ukf_map*. The mean trajectory error of the *ekf_map* and of the *ukf_map* were $0.89m$ and $0.87m$, respectively. And $0.48m$ and $0.45m$ for the standard deviations. Since the difference between both trajectory errors seems to be very small, the EKF was maintained in the architecture because it is simpler and faster than the UKF.
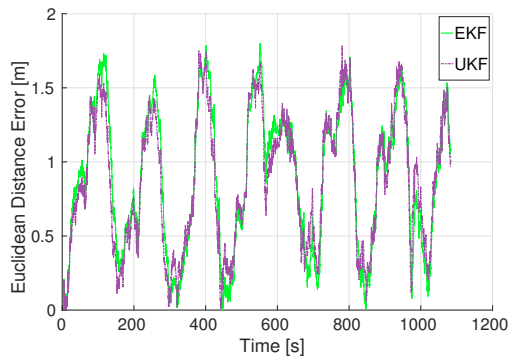

Fig. 9. Trajectory error of the EKF and the UKF.

4. CONCLUSIONS

The integration of an USBL system in the multi-sensor navigation module of AUVs increases considerably its localization accuracy and precision, hence its navigation and control performance. The navigation module presented in this paper implements two parallel EKFs, one integrating a DVL, an IMU and a pressure sensor, and the other

including all these aforementioned instruments plus a GPS and an USBL. The USBL delayed measurement is using odometric information before being integrated in an absolute EKF filter. Two different types of experiments have been carried out to support our approach: a) the USBL measurement precision obtained at several static positions decreases with the distance, with a standard deviation of $\sigma = 0.45m$ in a trajectory of $100m$; this precision calibration provides a better insight of how dispersed are the USBL measurements and thus how to approximate their covariance for the second localization filter; b) the assessment of the vehicle global position estimated by an absolute EKF, using an stereo SLAM approach as a GT, shows a trajectory error bounded in the range of $[0, 1.7]m$ in a route of $270m$, while the odometric error grows boundless. Finally, to keep the approach fast and simple, EKF seems to be a suitable filtering option.

REFERENCES

Guerrero, E., Massot, M., Negre, P.L., Bonin-Font, F., and Oliver., G. (2016). An USBL-Aided Multisensor Navigation System for Field AUVs. In *Proc. of the IEEE International Conference on Multisensor Fusion and Integration for Intelligent Systems (MFI)*.

Julier, S. and Uhlmann, J. (1997). A New Extension of the Kalman Filter to Nonlinear Systems. *Int. Symp Aerospace/Defense Sensing, Simulations and Controls*, 3, 182–193.

Moore, T. and Stouch, D. (2016). A Generalized Extended Kalman Filter Implementation for the Robot Operating System. *Advances in Intelligent Systems and Computing*, 302, 335–348. doi:10.1007/978-3-319-08338-4_25.

Negre, P.L., Bonin-Font, F., and Oliver, G. (2016). Cluster-Based Loop Closing Detection for Underwater SLAM in Feature-Poor Regions. In *Proc. of IEEE International Conference on Robotics and Automation (ICRA)*.

Negre, P. and Guerrero, E. (2016). SRV USBL ROS library. URL https://github.com/srv/acoustic_link,https://github.com/srv/usbl_position.

Quigley, M., Conley, K., Gerkey, B., Faust, J., Foote, T., Leibs, J., Wheeler, R., and Ng, A.Y. (2009). ROS: an Open Source Robot Operating System. In *ICRA Workshop on Open Source Software*.

Ribas, D., Ridao, P., Mallios, A., and Palomeras, N. (2012). Delayed State Information Filter for USBL-Aided AUV Navigation. In *Proc. of IEEE International Conference on Robotics and Automation (ICRA)*. Minnesota (USA).

Rigby, P., Pizarro, O., and Williams, S. (2006). Towards Geo-Referenced AUV Navigation Through Fusion of USBL and DVL Measurements. In *Proc. of IEEE Oceans*.

Stanway, M. (2010). Delayed-state Sigma Point Kalman Filters for Underwater Navigation. In *Proc. of the 13th IEEE/OES Autonomous Underwater Vehicles (AUV)*.

Sun, D., Zheng, C., Yeng, J., and Wu, Y. (2014). Initial Study on the Precision Evaluation for Ultra Short Baseline Positioning System. In *Proceedings of IEEE Oceans*.

Willemenot, E., Morvan, P., Pelletier, H., and Hoof, A. (2009). Subsea Positioning by Merging Inertial and Acoustic Technologies. In *Proceedings of IEEE Oceans*.